Amplification Maps for Syrian Territory with Respect to Ground Motion Levels and Based on Slope Angle-Velocity Model

Raed Ali Ahmad

Professor, National Earthquake Center, Damascus, Syria, email: raedali_2000@yahoo.com

Received: 05/03/2015
Accepted: 16/12/2015

ABSTRACT

In this paper, the ASTER Digital elevation model (DEM) corresponding to 30×30 m data spacing (medium resolution) is used to produce slope steepness, slope variations in the Syrian territory. The topographic slope corresponding to time-averaged shear wave velocity model (Vs^{30}) developed by Allen and Wald [1] has been used to derive empirical formula, and then to generate base data of Vs^{30} map for the Syrian territory. We have found that the values of Vs^{30} vary between Vs^{30} 180 to 760 m/s and fit the geological and topographic setting of Syria. Site-specific amplification factors (Fa and Fv) maps have been estimated with respect to the empirical equations proposed by Borcherdt [2]. The value of short-period amplification factor Fa varies from 0.91 to 1.85, while the value of mid-period Fv lies in the range 1.16 - 3.15. Comparing the estimated values of amplification factors for the Syrian territory shows a good similarity to those assigned in IBC-2006 for the same site-class. The acceleration-independent amplification factor F found to be changing from 1.38 to 5.83. The reclassified amplification factor F map shows clearly the areas with high potential for amplifying ground motion. The obtained maps are highly required by the Syrian anti-seismic design code. These maps have stored numerically with a resolution of 30×30 m. The results show that the slope angle-velocity model is an applicable technique for estimating seismic surface shear wave velocity (Vs^{30}). Image processing and remote sensing data, as well as digital elevation model can be used successfully to derive amplification maps.

Keywords:
Topographic slope; Time-averaged shear velocity; Amplification factors; Syria

1. Introduction

The current work presents the amplification maps with respect to the ground motion intensity (*I*) for Syrian territory for the first time. The aim of this work is estimating the site-specific amplification using satellite images especially the digital elevation model products. Image processing and remote sensing data, as well as digital elevation model can be used successfully to derive amplification maps, especially if the resolution of DEM and remote sensing images are medium. The manuscript presents a new way for preparation of spectral amplification maps of Syria using the slope angle-velocity model and with respect to ground motion intensity. The amplification maps are very important for civil engineers to calculate the total shear forces when designing infrastructure.

Image processing followed in the present work includes four major steps; 1) Making digital elevation model from remote sensing data or downloading them from proper website and recombine them in one image; 2) Creating a slope-angle image with 3×3 matrix of pixels using maximum squared technique;

3) Applying derived empirical equation to determine the time-averaged shear velocity on each pixel; 4) applying various amplification equations on each pixel of an image size. Classified image of general amplification factor is generated. We have written programs in *C* language to calculate slope, shear velocity, and predominant period output images from digital elevation model image (ASTER satellite). We have also used ArcGIS software to produce final images.

Estimation of ground motion severity at different site-condition is essential for anti-seismic design as well as for seismic safety analysis. Mapping seismic site-condition provides a great importance for recognition of ground-motion amplification [3-5]. An alternative method has proposed by Wald and Allen [6] for evaluating global seismic site conditions, or the time-averaged shear velocity to 30 m depth (Vs^{30}), from the Shuttle Radar Topography Mission (SRTM) 30 arcsec ($\approx 1\times1$ km) digital elevation models (DEMs). This method is developed for two sets of coefficients for predicting Vs^{30}: one for active tectonic regions that possess dynamic topographic relief, and one for stable continental regions where changes in topography are more subdued. The application of the topographic slope-velocity method in regions with abundant Vs^{30} measurements indicates that this method provides site condition-maps of similar quality, or in some cases, maps superior to those developed from more traditional techniques [1]. The maps derived from the slope-velocity model often well correlated with other independently derived, regional-scale site-condition maps. The slope-based method provides a simple approach to uniform site-condition mapping [6]. The topographic slope can be used as a reliable proxy for Vs^{30} in the absence of geological and geotechnical based site-condition maps through correlations between Vs^{30} measurements and topographic gradient [7].

A comparison between steeper topographic slopes and recent seismicity shows a great match. The current active tectonism and the topographic relief in the Middle East region is correlated one to one feature. The distribution of earthquake epicenters shows that earthquakes occur where the slope angle and topography are high. It is also noticed that the slightly difference in topography might reflect the soil condition and the boundary of major tectonic feature. A correlation of topographic slope with surface wave velocity (Vs^{30}) shows a great match. Using medium resolution (30×30 m) of DEM data could estimate finer-scale variations in topographic gradient. This is much better to correlate the velocity-slope angle model to geological and geomorphic features. Recent studies have confirmed good correlations between Vs^{30} and both slope and geomorphic indicators in Japan [8], and elevation with Vs^{30} in Taiwan [9]. Consequently, topographic variations should be an indicator of near-surface geomorphology and lithology to the first order, with steep mountains indicating rock, nearly flat basins indicating soil, and a transition between the end members on intermediate slopes. In addition, the topographic slope should be compatible with shear wave velocity (Vs^{30}), amplification, and predominant period of surface soil. High-velocity materials are more likely to maintain a steep slope whereas basin sediments are deposited primarily in environments with very low gradients and described by low shear-wave velocity.

Many of the ground motion prediction equations [9-10] are calibrated against seismic station site conditions described with Vs^{30} values. As well, various scientists have shown various attenuation relations for numerous countries [11-13] based on peak ground or spectral accelerations. Different site conditions can induce amplifications of different period ranges in the response spectra [14-15]. A building may be more severely damaged if the natural periods of the structure happen to be close to the amplified periods of the ground [16-18]. Therefore, the local site conditions become important in ground motion analysis and in earthquake resistant designs. An earthquake response spectrum compatible with local site condition, anchoring to appropriate peak ground acceleration (PGA), is a common input for structural dynamic analysis [19-21]. The geologic condition at a site is commonly restricted to the upper-most layers. Anderson et al. [22] have found that the surficial geology (upper 30 m) has a greater influence on ground motions compared to thickness of layers, criteria for site classification based on near-surface properties alone are incomplete. They recommended the use of spectral decay parameter (k) and observed resonant frequencies, in addition to Vs^{30}, to characterize sites where 1D modeling is appropriate. Because quantitative subsurface soil properties are not commonly

Table 1a. The values of short-period amplification factor *Fa* for different site-class [26]. S_s is the cutoff input peak acceleration in g.

Site Class	$S_S \leq 0.25$	$S_S = 0.5$	$S_S = 0.75$	$S_S = 1.00$	$S_S \geq 1.25$
A	0.8	0.8	0.8	0.8	0.8
B	1.0	1.0	1.0	1.0	1.0
C	1.2	1.2	1.1	1.0	1.0
D	1.6	1.4	1.2	1.1	1.0
E	2.5	1.7	1.2	0.9	0.9

Table 1b. The values of mid-period amplification factor *Fv* for different site-class [26]. S_s is the cutoff input peak acceleration in g.

Site Class	$S_S \leq 0.25$	$S_S = 0.5$	$S_S = 0.75$	$S_S = 1.00$	$S_S \geq 1.25$
A	0.8	0.8	0.8	0.8	0.8
B	1.0	1.0	1.0	1.0	1.0
C	1.7	1.6	1.5	1.4	1.3
D	2.4	2.0	1.8	1.6	1.5
E	3.5	3.2	2.8	2.4	2.4

available for every site, the use of surface geology becomes important in understanding the subsurface geologic conditions. Empirical relationships between the surface geology and the subsurface shear-wave velocity have been developed and are used in ground motion amplification predictions [3, 23, 24, 25]. Various versions of the international building codes (e.g., [26]) have assigned the values of amplification factors of *Fa* and *Fv* for each site-class with respect to the various ground motion levels of acceleration, Tables (1-a) and (1b).

2. Study Area

Syria lies between latitude 32.3° to 37.4°N and longitude 34.5° to 42.5° E and covers an area of about 185,180 km^2. Syria is located in southwestern Asia, north of the Arabian peninsula in the Middle East, at the eastern end of the Mediterranean sea. It consists of mountain ranges in the west and farther inland a steppe area. In the east is the Syrian desert and in the south is the Jabal al-Arab. The highest point in Syria is mount Hermon (2,814 m) on the Lebanese border, lowest point: unnamed location near Lake Tiberias -200 m.

In Syria, perhaps instrumental seismicity is low to moderate; most of earthquakes occur along Dead Sea Fault System (DSFS), Palmyride fold belt and Abd el Aziz-Sinjar uplifts [27]. Dead Sea Fault System plays an important role in Syrian seismicity. Many destructive earthquakes occurred along Dead Sea Fault causing severe damage in Syria and neighboring countries. Historical documents provide an account of damaging earthquakes occurred in the years 1157, 1170, 1202, 1408, and 1837. Figure (1) shows Syrian seismicity catalog for the period of 1365 BC till 2014 AC plotted on digital elevation image.

The plate boundary processes affect the overall tectonics of the Syrian territory and are mainly responsible for the structure and kinematics in the study area and Middle East region, including the intraplate processes. In a general sense, the dynamic plate boundary processes in Syria and surrounding countries are manifested in the present day topography [28]. Higher topography and relief in the region coincide mainly with plate collision zones such as the Zagros. Distinct topographic features are also observed along DSFS and other tectonic features in Syria. A correlation of steeper topographic slopes and recent seismicity are observed. Topography variations to some extent reflect the seismic activity in the region. Higher topography is an indication of seismicity of the area. Intuitively, the topography variations in sedimentary basin might reflect the seismic activity in the area, especially when it is accompanied with the existence of earthquake epicenters.

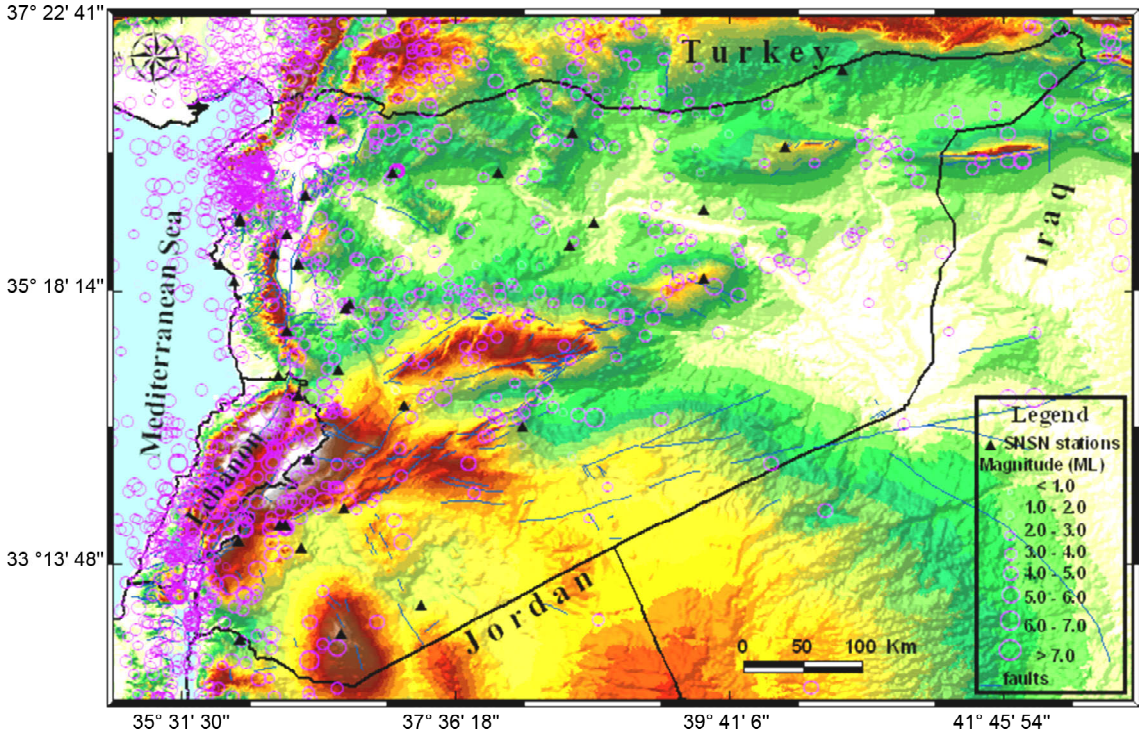

Figure 1. Syrian seismicity catalog for the period of 1365 BC till 2015 AC plotted on digital elevation image, black triangles represent the Syrian seismological stations.

3. Digital Elevation Model (DEM)

ASTER data is used for generation of digital elevation models, slope and hazard monitoring. The ASTER DEM data corresponding to 30×30 m data spacing is used to produce slope steepness and slope variations in the study area. Digital elevation models are data files that contain the elevation of the terrain over a specified area, usually at a fixed grid interval over the "Bare Earth". The intervals between each grid points will always be referenced to some geographical coordinate system. Quality DEM products are measured by how accurate the elevation is at each pixel and how accurately the morphology is presented. Several factors are important for the quality of DEM-derived products: terrain roughness, sampling density (elevation data collection method), grid resolution or pixel size, interpolation algorithm, vertical resolution and terrain analysis algorithm. The common uses of DEMs include: extracting terrain parameters, modeling water flow or mass movement, creation of relief maps, rendering of 3D visualizations, creation of physical models (including raised-relief maps), rectification of aerial photography or satellite imagery, reduction (terrain correction) of gravity measurements (gravimetry, physical geodesy) and terrain analyses in geomorphology and physical geography. The digital elevation image has been generated for Syria and the surrounding countries as seen in Figure (2).

4. Topographic Slope

For each cell, slope calculates the maximum rate of change in value from that cell to its neighbors. Basically, the maximum change in elevation over the distance between the cell and its eight neighbors identifies the steepest downhill descent from the cell. Conceptually, the Slope function fits a plane to the z-values of a 3×3 cell neighborhood around the processing or center cell. The slope value of this plane is calculated using the average maximum technique. The direction that the plane faces is the aspect for the processing cell. The lower the slope value, the flatter the terrain is; the higher the slope value, the steeper the terrain is. Based on the slope function mentioned above, the slope image has been produced for the study area using the ASTER-DEM image data with resolution 30×30 m as seen in Figure (3). The slopes are calculated in degrees, using average maximum technique.

5. Slope Angle-Velocity Model

In this work, the velocity-slope model proposed by Allen and Wald [1] has been used to produce empirical formula. The unit of slope ranges has converted to degree and then the values of velocity were calculated for each pixel size. The study area has divided into several files for simple calculation. Image processing followed in the present work includes four major steps; making digital elevation model from remote sensing data or downloading

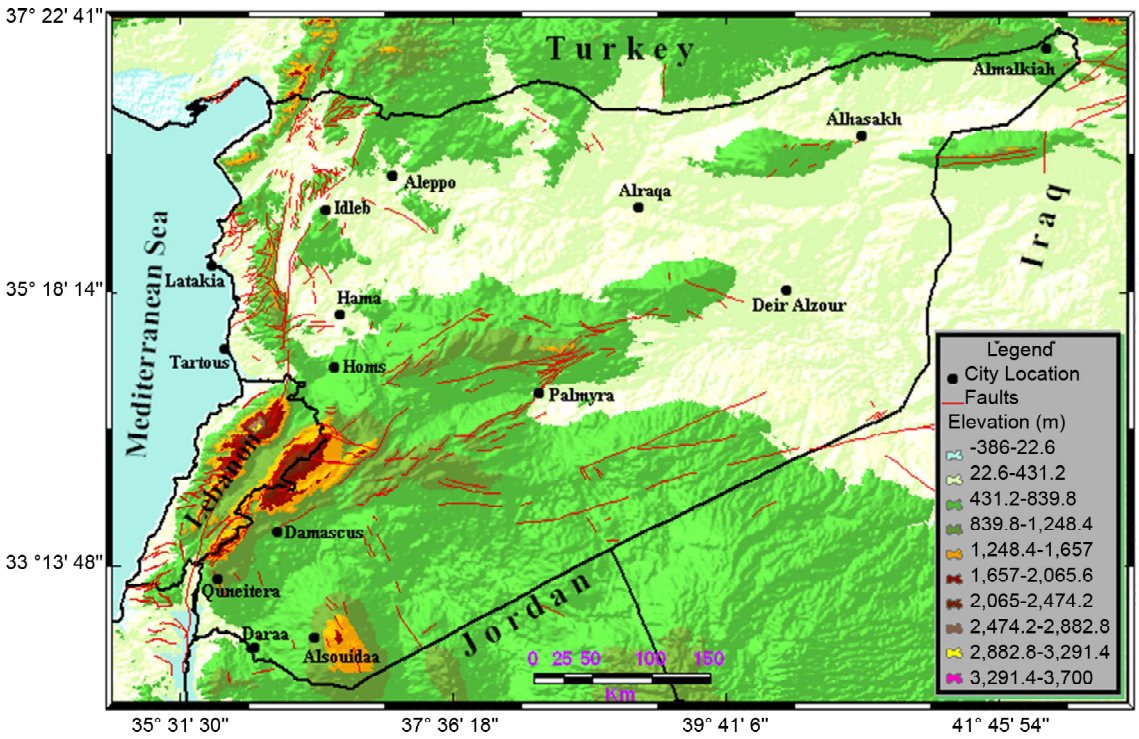

Figure 2. Classified DEM image produced for study area using Aster data and overlaid by tectonic features.

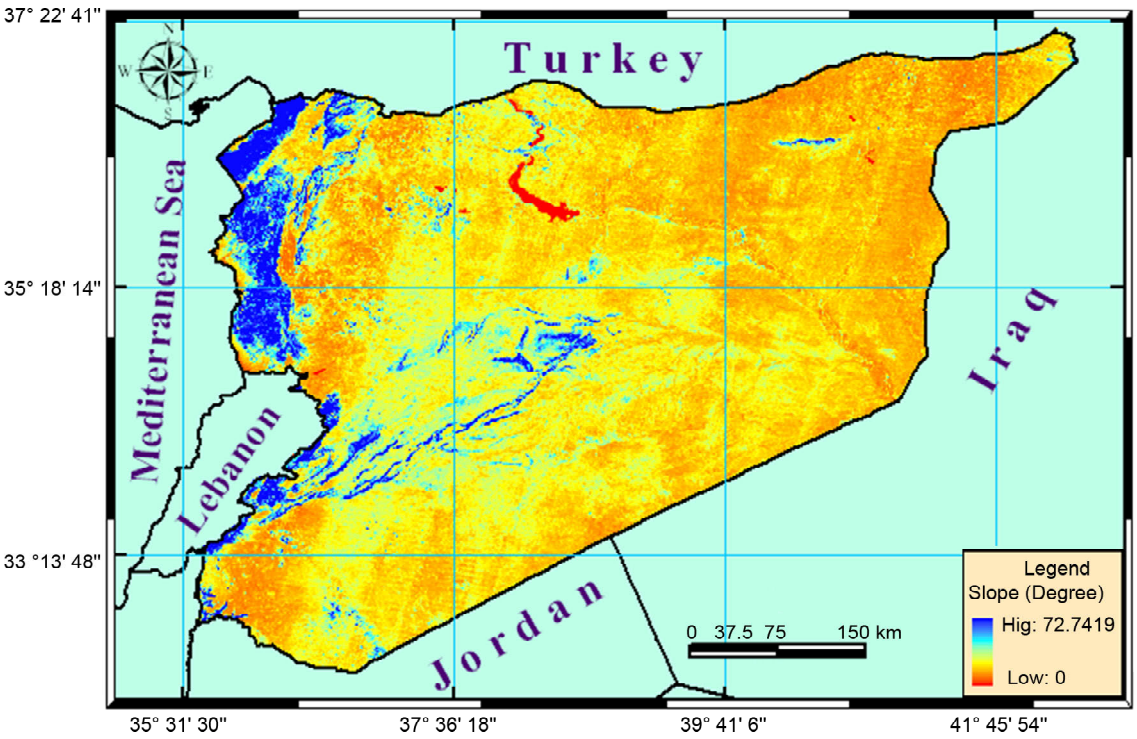

Figure 3. The slope variations image of the study area.

them from proper website and recombine them in one image; creating slope-angle image from 3×3 matrix of pixels using maximum squared technique; applying derived empirical equation to determine the shear velocity on each pixel, applying various amplification equations on each pixel of an image size. We have written some programs in *C* language to calculate slope, shear velocity, and predominant period output images from digital elevation model image (ASTER satellite). We have also used ArcGIS software to produce final images.

Based on Wald and Allen [6] method and the corresponded slope values (degree) estimated from slope image at various locations of Syria, an empirical formula is produced that correlates the slope angle with shear velocity. This formula is:

$Vs^{30} = 369.6\ S_r^{0.2515}$ where S_r: slope in degree. If $S_r = 0°$ then $Vs^{30} = 180$; if $S_r \geq 18°$ then $Vs^{30} = 760$.

This formula has been applied to produce the base shear velocity Vs^{30} image and then we calculated various amplification factors for each pixel of an Vs^{30} image to produce the amplification images for short and mid-periods. Figure (4) shows the produced Vs^{30} map for the study area.

6. Amplification Factors

The amplification factors *Fa* and *Fv* for short- and mid-period motion may be predicted as a function of time-averaged shear-wave velocity *v* for various input ground-motion levels, *I*, with respect to a reference ground condition by the following equations

$$F_a(v, I_a) = (v_o / v)^{m_a} \tag{1}$$

and

$$F_v(v, I_a) = (v_o / v)^{m_v} \tag{2}$$

where

$$m_a = Log[F_a(v_{SC-IV}, I_a)] / Log[v_o / v_{SC-IV}]$$
$$m_v = Log[F_v(v_{SC-IV}, I_a)] / Log[v_o / v_{SC-IV}] \tag{3}$$

v_{SC-IV} is time-averaged shear velocity for the site class [2].

The general amplification factor *F* for any site and without any respect to ground motion *I*, could be predicted as:

$$F = v_o / v$$

where v_o is the time-averaged shear velocity of rocky medium $v_o \approx 1050 m/s$.

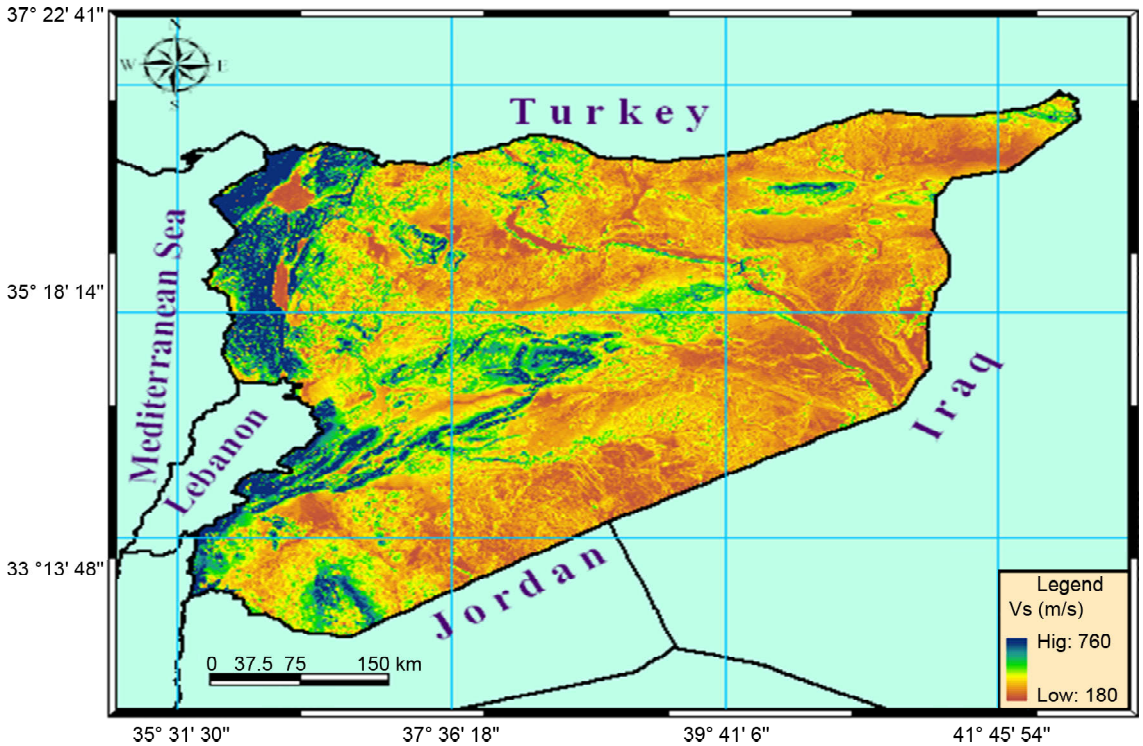

Figure 4. The surface shear-wave velocity V_S^{30} map of study area.

Based on the produced velocity map, the maps of amplification factors of *F*, *Fa* and *Fv* could be estimated for Syrian territory with respect to the ground motion levels of 0.1, 0.2, 0.3 and 0.4 g. The results are shown in Figures (5), (6) and (7). The general amplification *F* map is created using the direct estimation of the average velocity of the rock divided by the value of surface velocity of the soil for each pixel size. Based on the values of *F*, the Syrian area was classified into five categories: very low (1.28-2.27), low (2.27-3.16), averaged (3.16-4.05), intermediate (4.05-4.94) and high (4.94-5.83). The classified map of *F* shows clearly the areas of high and low amplification, as seen in Figure (7) (right).

7. Amplification Factors along Damascus Basin

The Damascus basin, which covers a total area of about 8,692 km^2 , is located in the south-western part of Syria and lies between 32°43' and 33°55' of latitude *N* and 35°48' and 37° 05' of longitude *E*. As a result of a series of tectonic, volcanic and weathering events, which already started in the late Mesozoic period, several fold structures appeared, such as the mount Anti-Lebanon [up to 2,466 m above sea level], mount Hermon (2,814 m), Palmyrides (1,308 m) and mount Arab (1,790 m). The altitude of the so-called "Damascus Ghotta basin" which occupies the flat central part between the above-mentioned fold mountains, ranges between 710 m at the foothill of mount Qassyoun and 588 m at the Al Hijaneh area [29]. From a geological point of view, the Damascus basin is situated at the junction between two major structures: the mount Arab depression in the south; and the Palmyrides-fold system, which includes also the mount Anti-Lebanon, in the north and west. Consequently, the so-called "Damascus depression" as a structure

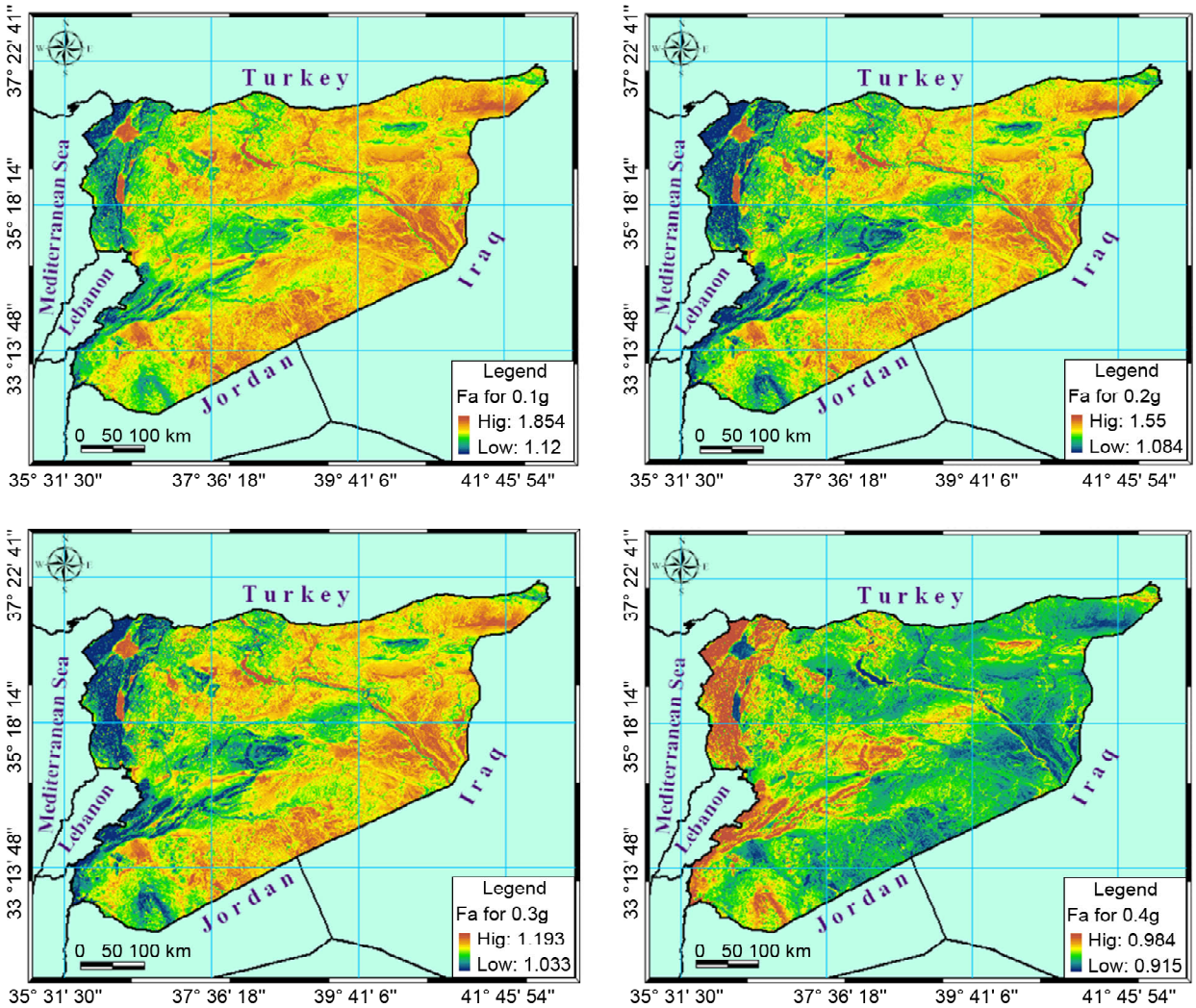

Figure 5. Short-period *Fa* amplification factor maps made for Syrian territory for specified levels of input ground motion 0.1, 0.2, 0.3 and 0.4 g.

occupying the central zone, forms a geologic syncline filled with continental and lacustrine deposits and volcanic lavas. Accordingly, the stratigraphic sequence in the Damascus basin is represented by the Jurassic, Cretaceous, Paleogene, Neogene and Quaternary deposits [29].

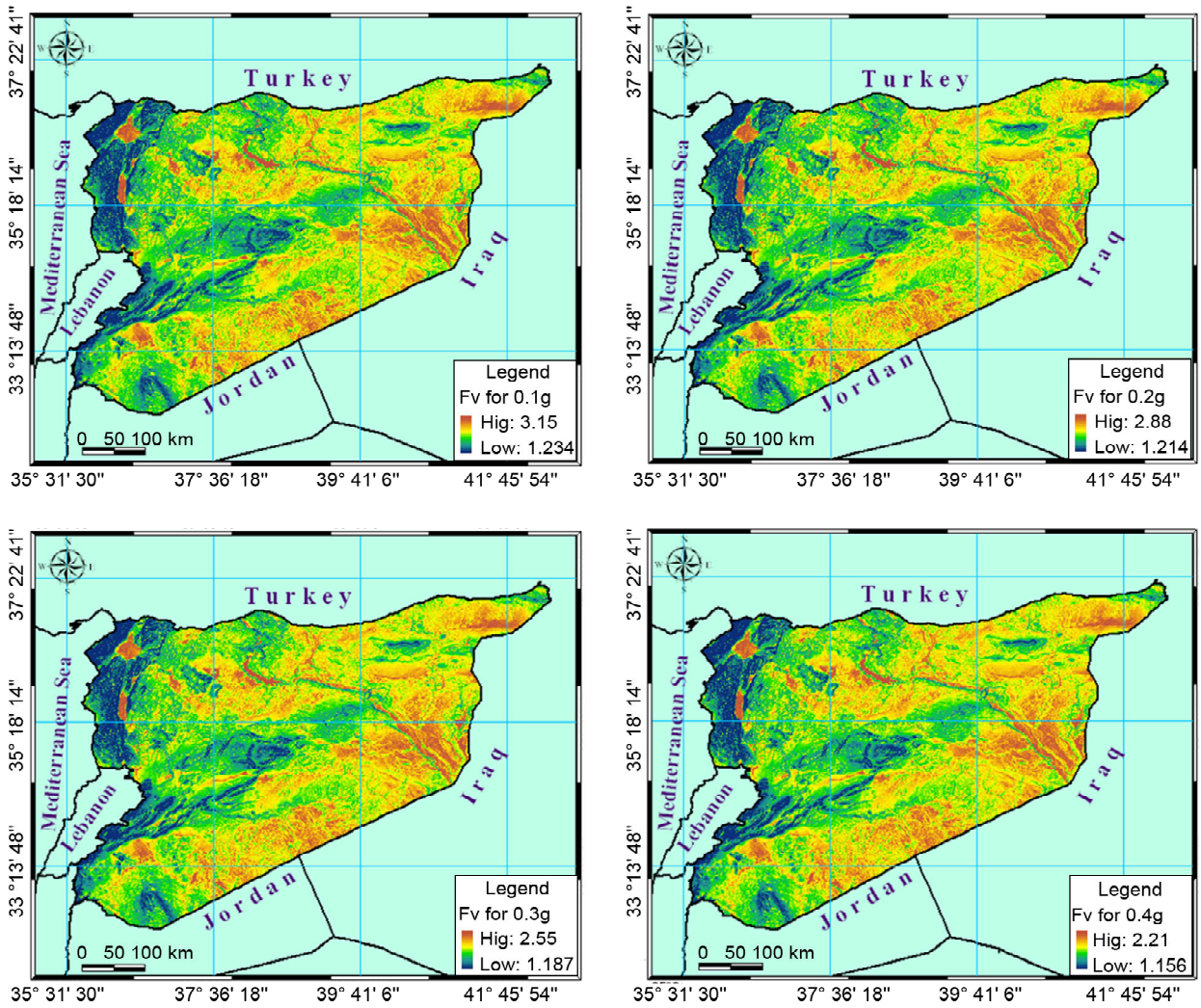

Figure 6. Mid-period Fv amplification factor maps made for Syrian territory for specified levels of input ground motion 0.1, 0.2, 0.3 and 0.4 g.

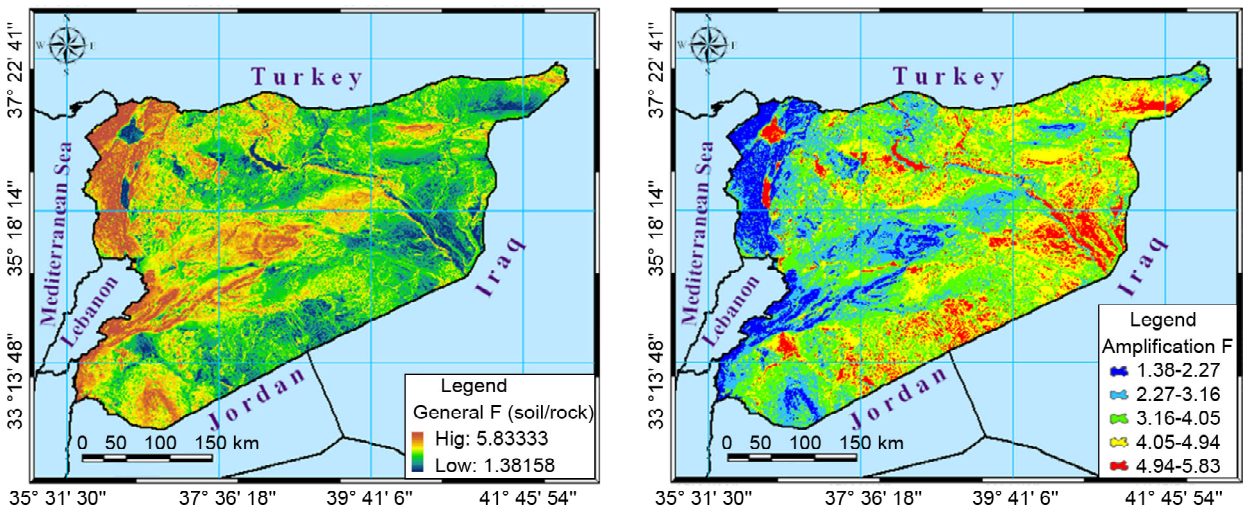

Figure 7. The general amplification factor F map made for Syrian territory without respect to the ground motion levels (left) and it's classified image (right).

Since the output images are stored numerically, one can take any profile to measure the variation of amplification factors, elevation, and velocity. Firstly, we have chosen two points of *A* and *B* along Damascus basin. "*A*" is located at the coordinates of 36.2984° E and 33.372° N, while "*B*" takes the following coordinates of 36.752° E and 33.654° N. Figure (8) shows the location of profile A-B drawn on draped velocity (V_S^{30}) map of the region along Damascus basin. The changes in amplification factors of *F*, *Fa* and *Fv* along A-B profile could be easily estimated. The profile A-B is trending south-west to north-east direction of Damascus city. The variations in the amplification factors along profile A-B is shown in Figure (9). The general amplification factor "*F*" classified image shows that Damascus

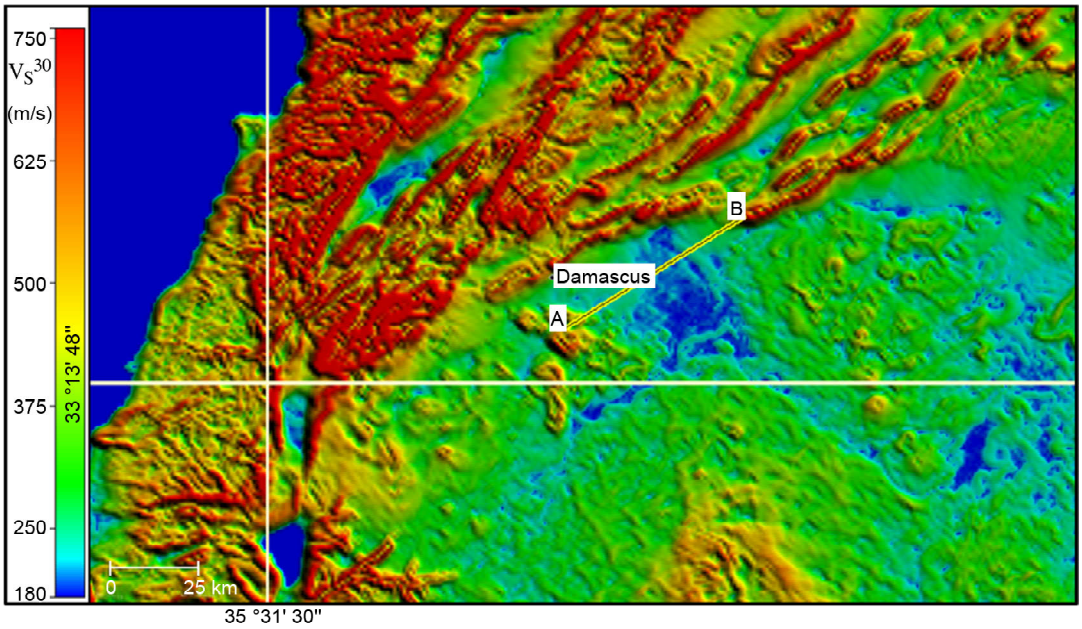

Figure 8. Draped velocity image showing the profile A-B along Damascus basin.

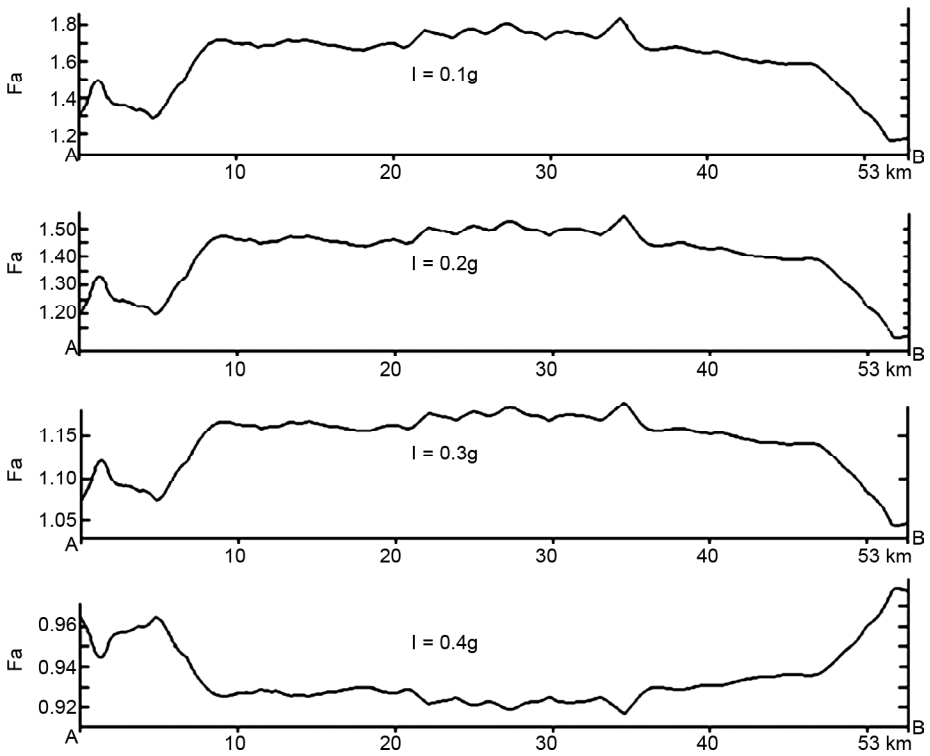

Figure 9. Changes in short-period amplification factor Fa along profile A-B with respect to the ground motion levels of 0.1, 0.2, 0.3 and 0.4 g.

basin is dominated by a high-amplification value from 4.05 to 5.83. This factor is decreased to reach 3.16 near the foothill of mount Qasioun. Steep topography has lesser value of the amplification factor "*F*".

The changes in various amplification factors of *F*, *Fa*, and *Fv* along profile A-B are shown in Figures (9) to (11). The results show that the maximum amplification found to be around 3.15 for the ground level of 0.1 g for mid-period of 0.5-2 s. The minimum short-period amplification found to be 0.92 for the ground motion level of 0.4 g. Damascus basin reduces the ground motion level for strong earthquake with PGA ≥ 0.4 g. The sediments in the Damascus basin always amplify the ground motion parameters for lower acceleration of 0.4 g. The value of general amplification *F* factor varies from 1.5 to 5.8. The effect of Damascus basin is manifested and directly shown from amplification curves. For mid-periods, the amplification factors always decrease towards southern part of Palmyride fold belt near the location of point "B". A comparison of amplification factors with slope, elevation, and velocity have shown a great match. The Damascus basin can be characterized by low to medium shear wave velocity, low slope angle 3° to 7°, and low elevation area less than 650 m. Figure (12) shows the comparison of slope, elevation and V_s^{30} along A-B profile along Damascus basin.

The results estimated using remote sensing and digital elevation model is compared to the results estimated from previous field work done by Zaineh et al. [30] for Damascus area. Zaineh et al. [30] estimated the average short period Fa (0.05-0.5 s) amplification factor using array measurements of microtremors for thirty sites in Damascus region. Based on his results, the estimated short period amplification factor varies in the range 2.1-3.8. He

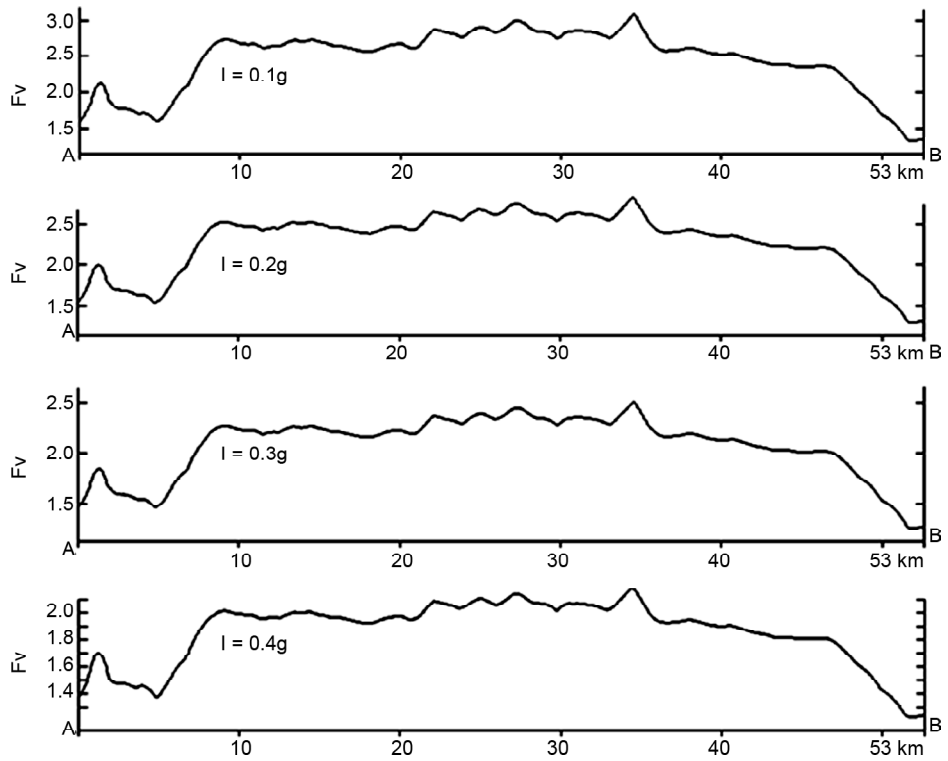

Figure 10. Changes in mid-period amplification factor *Fv* along profile A-B with respect to the ground motion levels of 0.1, 0.2, 0.3 and 0.4 g.

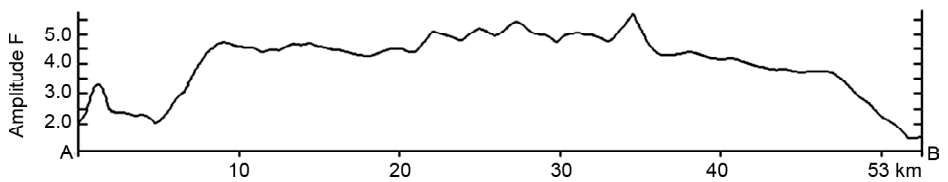

Figure 11. Changes in general amplification factor*F* (hard-rock to soil) along A-B profile.

also estimated the shear velocity up to 30 m for the same thirty sites. The V_s^{30} velocity value varies in the range 301-592 m/s. His measured elevation, amplification and velocity data have used for comparison. In order to compare his obtained data, the Borcherdt [2] amplification factors *Fa* and *Fv* were computed, and a very close agreements to his field results were found. The calculated averaged standard deviations are: 2.38 m, 32.4 m/s and 0.46 for the elevation, velocity V_s^{30} and general amplification (*F*) respectively. The mean STD value for the short and mid period is 0.065 as maximum, Table (2). Tables (3) and (4) present various used parameters calculations. In comparison to Borcherdt amplifica-

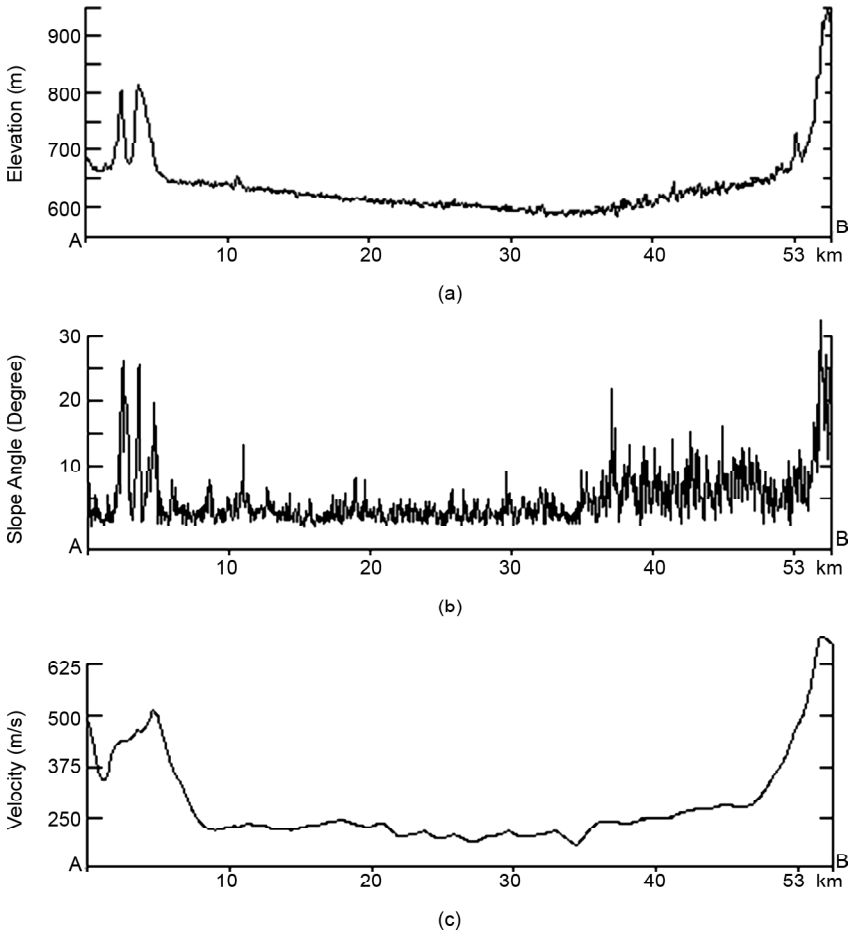

Figure 12. a) topography, (b) slope angle, and (c) velocity Vs30 variations along profile A-B.

Table 2. Comparison of estimated results from image processing method and field work done by Zaineh et al. [30] in Damascus region.

Using ASTER DEM and Image Processing Method Presented in This Work											
The Averaged Value (Only) of the 30 Sites in Damascus Region				Short Period Amplification				Mid-Period Amplification			
Elev. (m)	Slope	Vs^{30} (m/s)	*F*	*Fa* 0.1	*Fa* 0.2	*Fa* 0.3	*Fa* 0.4	*Fv* 0.1	*Fv* 0.2	*Fv* 0.3	*Fv* 0.4
698.4	4.667	523.04	2.096	1.286	1.196	1.074	0.965	1.6	1.543	1.466	1.383
Using the Results Reported by Zaineh et al. [30] Based on Array H/V Measurements											
The Averaged Value (Only) of the 30 Sites in Damascus Region				Short Period Amplification				Mid-Period Amplification			
Elev. (m)	Vs^{30} (m/s)	*F* (0.05 – 0.5s) (II/V)		*Fa* I=0.1g	*Fa* 0.2g	*Fa* 0.3g	*Fa* 0.4	*Fv* 0.1	*Fv* 0.2	*Fv* 0.3g	*Fv* 0.4 g
703.17	458.24	3.0241		1.348	1.237	1.089	0.959	1.748	1.673	1.575	1.469
The Averaged Standard Deviation (STD) between Field and Image Processing Methods											
2.38	**32.4**	**0.464**	**0.031**	**0.041**	**0.0075**	**0.003**	**0.036**	**0.065**	**0.054**	**0.043**	

Table 3. The estimated elevation, slope, V_s^{30}, and the amplification factors using ASTER DEM image processing method.

Long. (°)	Lat. (°)	Elevation DEM (m)	Slope (°)	Vs^{30} (m/s)	F	Fa I=0.1g	Fa 0.2g	Fa 0.3g	Fa 0.4g	Fv 0.1g	Fv 0.2g	Fv 0.3g	Fv 0.4
36.425	33.437	625.000	2.540	467.233	2.269	1.328	1.224	1.084	0.960	1.693	1.626	1.536	1.440
36.401	33.484	640.000	7.097	605.031	1.753	1.213	1.148	1.057	0.973	1.431	1.392	1.339	1.282
36.402	33.537	641.000	4.948	552.572	1.919	1.252	1.174	1.066	0.968	1.518	1.470	1.405	1.335
36.389	33.512	650.000	3.480	505.738	2.097	1.291	1.200	1.076	0.964	1.608	1.550	1.473	1.389
36.353	33.419	651.000	2.750	476.659	2.225	1.318	1.218	1.082	0.961	1.671	1.606	1.520	1.427
36.397	33.564	657.000	2.849	480.924	2.205	1.314	1.216	1.081	0.962	1.661	1.598	1.513	1.421
36.327	33.442	656.000	5.654	571.421	1.856	1.237	1.164	1.063	0.970	1.485	1.441	1.381	1.315
36.351	33.487	659.000	2.428	461.972	2.295	1.333	1.228	1.086	0.960	1.705	1.637	1.545	1.447
36.326	33.471	662.000	3.283	498.391	2.128	1.298	1.205	1.077	0.963	1.623	1.564	1.484	1.398
36.294	33.440	666.000	4.066	525.955	2.016	1.274	1.189	1.072	0.966	1.567	1.514	1.443	1.365
36.358	33.525	672.000	6.129	583.135	1.818	1.229	1.158	1.061	0.971	1.466	1.423	1.366	1.303
36.316	33.509	684.000	5.365	563.919	1.880	1.243	1.168	1.064	0.969	1.498	1.452	1.390	1.323
36.260	33.441	683.000	4.847	549.705	1.929	1.254	1.176	1.067	0.968	1.523	1.474	1.409	1.338
36.320	33.522	686.000	7.043	603.869	1.756	1.214	1.148	1.057	0.973	1.433	1.394	1.341	1.283
36.298	33.479	676.000	1.492	408.727	2.594	1.391	1.266	1.099	0.954	1.846	1.761	1.649	1.529
36.299	33.513	691.000	0.746	343.355	3.088	1.479	1.322	1.118	0.946	2.068	1.956	1.808	1.654
36.307	33.512	684.000	0.667	333.855	3.176	1.493	1.332	1.121	0.944	2.106	1.989	1.835	1.675
36.307	33.510	693.000	3.998	523.709	2.025	1.276	1.190	1.072	0.966	1.572	1.518	1.446	1.368
36.309	33.527	687.000	4.767	547.399	1.937	1.256	1.177	1.067	0.968	1.527	1.478	1.412	1.341
36.364	33.553	695.000	8.304	629.403	1.685	1.196	1.136	1.053	0.975	1.395	1.359	1.312	1.259
36.253	33.484	699.000	1.796	428.267	2.476	1.369	1.251	1.094	0.956	1.791	1.713	1.609	1.497
36.227	33.460	701.000	1.376	400.462	2.648	1.401	1.272	1.101	0.953	1.871	1.783	1.667	1.543
36.217	33.434	709.000	7.004	603.030	1.758	1.214	1.149	1.057	0.973	1.434	1.395	1.342	1.283
36.284	33.511	695.000	2.428	461.972	2.295	1.333	1.228	1.086	0.960	1.705	1.637	1.545	1.447
36.368	33.585	709.000	1.945	436.913	2.427	1.359	1.245	1.092	0.957	1.768	1.692	1.592	1.484
36.342	33.545	729.000	7.565	614.828	1.725	1.206	1.143	1.055	0.974	1.416	1.379	1.328	1.272
36.252	33.505	737.000	9.174	645.386	1.643	1.186	1.129	1.050	0.976	1.372	1.339	1.294	1.245
36.304	33.548	821.000	11.521	683.440	1.551	1.162	1.113	1.044	0.979	1.322	1.294	1.256	1.213
36.277	33.533	1095.000	10.082	660.879	1.604	1.176	1.123	1.047	0.977	1.351	1.320	1.278	1.232
Mean		**698.379**	**4.667**	**523.040**	**2.096**	**1.286**	**1.196**	**1.074**	**0.965**	**1.601**	**1.543**	**1.466**	**1.383**

Table 4. The estimated elevation, V_s^{30}, and the amplification factors based on Zaineh et al. [30] field work.

Long. (°)	Lat. (°)	Elevation (m)	Vs^{30} (m/s)	F (0.05 - 0.5s)	Fa I=0.1g	Fa 0.2g	Fa 0.3g	Fa 0.4g	Fv 0.1g	Fv 0.2g	Fv 0.3g	Fv 0.4
36.425	33.437	634.000	338.000	2.900	1.487	1.328	1.120	0.945	2.089	1.974	1.823	1.665
36.401	33.484	647.000	304.000	3.000	1.543	1.363	1.132	0.940	2.238	2.104	1.929	1.747
36.402	33.537	649.000	334.000	3.100	1.493	1.332	1.121	0.944	2.105	1.988	1.835	1.674
36.389	33.512	652.000	387.000	3.500	1.418	1.283	1.105	0.951	1.913	1.820	1.697	1.567
36.353	33.419	654.000	400.000	2.900	1.402	1.273	1.101	0.953	1.873	1.784	1.668	1.544
36.397	33.564	657.000	380.000	3.500	1.427	1.289	1.107	0.950	1.936	1.840	1.714	1.580
36.327	33.442	659.000	500.000	2.100	1.297	1.204	1.077	0.964	1.620	1.561	1.482	1.396
36.351	33.487	665.000	384.000	3.300	1.422	1.286	1.106	0.951	1.923	1.829	1.704	1.572
36.326	33.471	668.000	574.000	3.000	1.235	1.163	1.062	0.970	1.481	1.437	1.377	1.312
36.294	33.440	672.000	500.000	2.200	1.297	1.204	1.077	0.964	1.620	1.561	1.482	1.396
36.358	33.525	682.000	301.000	3.000	1.549	1.367	1.133	0.939	2.253	2.116	1.939	1.755
36.316	33.509	687.000	484.000	3.100	1.311	1.214	1.081	0.962	1.654	1.591	1.508	1.417
36.260	33.441	687.000	417.000	3.100	1.382	1.260	1.097	0.955	1.823	1.740	1.631	1.515
36.320	33.522	689.000	429.000	3.600	1.368	1.251	1.094	0.956	1.789	1.711	1.607	1.496
36.298	33.479	689.000	503.000	2.900	1.294	1.202	1.076	0.964	1.613	1.555	1.477	1.393
36.299	33.513	691.000	419.000	3.400	1.379	1.258	1.096	0.955	1.817	1.735	1.627	1.512

Table 4. Contine.

Long. (°)	Lat. (°)	Elevation (m)	Vs^{30} (m/s)	F (0.05 - 0.5s)	Fa 1=0.1g	Fa 0.2g	Fa 0.3g	Fa 0.4g	Fv 0.1g	Fv 0.2g	Fv 0.3g	Fv 0.4
36.299	33.513	691.000	419.000	3.400	1.379	1.258	1.096	0.955	1.817	1.735	1.627	1.512
36.307	33.512	694.000	433.000	2.900	1.363	1.248	1.093	0.957	1.779	1.701	1.599	1.490
36.307	33.510	697.000	484.000	3.100	1.311	1.214	1.081	0.962	1.654	1.591	1.508	1.417
36.309	33.527	697.000	399.000	3.300	1.403	1.274	1.102	0.953	1.876	1.787	1.670	1.546
36.364	33.553	701.000	455.000	3.600	1.340	1.233	1.087	0.959	1.722	1.652	1.558	1.457
36.253	33.484	703.000	455.000	2.600	1.340	1.233	1.087	0.959	1.722	1.652	1.558	1.457
36.227	33.460	706.000	515.000	2.700	1.283	1.195	1.074	0.965	1.589	1.533	1.459	1.378
36.217	33.434	708.000	588.000	3.800	1.225	1.156	1.060	0.971	1.458	1.416	1.360	1.298
36.284	33.511	710.000	592.000	3.000	1.222	1.154	1.059	0.972	1.451	1.410	1.355	1.294
36.368	33.585	714.000	495.000	2.900	1.301	1.207	1.078	0.963	1.630	1.570	1.490	1.403
36.342	33.545	723.000	570.000	2.400	1.238	1.165	1.063	0.970	1.487	1.443	1.382	1.316
36.252	33.505	740.000	515.000	2.700	1.283	1.195	1.074	0.965	1.589	1.533	1.459	1.378
36.304	33.548	809.000	542.000	3.000	1.260	1.180	1.068	0.967	1.537	1.487	1.420	1.347
36.277	33.533	1108.000	592.000	3.100	1.222	1.154	1.059	0.972	1.451	1.410	1.355	1.294
Mean		**703.172**	**458.241**	**3.024**	**1.348**	**1.237**	**1.089**	**0.959**	**1.748**	**1.674**	**1.575**	**1.470**

tion factors, it has been noticed that our proposed technique give better estimation of averaged *Fa* (2.096) than the array *H/V* method (*Fa* = 3.024).

8. Conclusions

The results presented here show the use of remote sensing data as well as digital elevation model (DEM) in evaluating the site-conditions and developing an amplification map. The results show that the slope angle-velocity model is an applicable technique for estimating the seismic surface shear wave velocity (V_s^{30}). Image processing and remote sensing data, as well as digital elevation model can be used successfully to derive the amplification maps.

Mapping seismic site condition provides a great importance to recognition of ground-motion amplification. The estimated results have proved that the velocity-slope angle model is compatible for estimating the shear wave velocity (V_s^{30}) and amplification. In general, the obtained maps fit the geological and geomorphological setting of Syria. The results show that the basins sediment in Syria are corresponded to high values of amplification factors and low shear wave velocity.

The derived maps are very much required by Syrian anti-seismic building code. These maps are done for the first time for the Syrian region. Site-specific amplification factors (*Fa* and *Fv*) maps have been estimated with respect to the empirical equations proposed by Borcherdt [2]. We have found that the value of V_s^{30} varies between 180 to 760 m/s and fit the geological and topographic setting of Syria. The amplification factors have computed for different ground motion levels of acceleration 0.1, 0.2, 0.3, and 0.4 g. The amplification factors of *Fa* value varies from 0.9156 to 1.854, while the value of *Fv* lies in the range of 1.156 to 3.146. The value of general amplification factor found to be changing from 1.381 to 5.83. The results show that the mean general amplification value for Syrian territory is around *F* = 3.9. The changes in the amplification factors along profile A-B of Damascus basin have been discussed. All maps have been stored numerically in high resolution image of 30×30 m.

Acknowledgments

The author would like to express his gratitude to anonymous referees and the Editor for their fruitful and valuable comments, which have helped me to improve earlier version of the manuscript. The author is grateful to the Japanese ASTER satellite for making DEM image available and for USGS website for providing the various valuable information. The author is grateful to Prof. Ramesh P. Singh, Chapman University, USA for his encouragement and support.

References

1. Allen, T.I. and Wald, D.J. (2007) *Topographic*

Slope as a Proxy for Seismic Site-Conditions (V_s^{30}) *and Amplification around the Globe*. U.S. Geol. Surv. Open-File Rept. 2007-1357, 69p.

2. Borcherdt, R.D. (1994) Estimates of site-dependent response spectra for design (methodology and justification). *Earthquake Spectra*, **10**, 617-653.

3. Park, S. and Elrick, S. (1998) Predictions of shear-wave velocities in southern California using surface geology. *Bull. Seism. Soc. Am.*, **88**, 677-685.

4. Wills, C. and Gutierrez, C. (2008) *Investigation of Geographic Rules for Improving Site-Conditions Mapping*. Calif. Geol. Surv. Final Tech. Rept., 20p. (Award No. 07HQGR0061).

5. Holzer, T.L., Padovani, A.C., Bennett, M.J., Noce, T.E., and Tinsley, J.C. III (2005) Mapping V_s^{30} site classes. *Earthquake Spectra*, **21**(2), 353-370.

6. Wald, D.J. and Allen, T.I. (2007) Topographic slope as a proxy for seismic site conditions and amplification. *Bull. Seismol. Soc. Am.*, 97, 1379-1395.

7. Allen, T.I. and Wald, D.J. (2009) On the use of high-resolution topographic data as a proxy for seismic site conditions (V_s^{30}). *Bull. Seism. Soc. Am.*, **99**(2A), 935-943.

8. Matsuoka, M., Wakamatsu, K., Fujimoto, K., and Midorikawa, S. (2005) Nationwide site amplification zoning using GIS-based Japan Engineering Geomorphologic Classification Map. *Proc. 9th Int. Conf. on Struct. Safety and Reliability*, 239-246.

9. Chiou, B.S.J. and Youngs, R.R. (2006) *PEER-NGA Empirical Ground Motion Model for the Average Horizontal Component of Peak Acceleration and Pseudo-Spectral Acceleration for Spectral Periods of 0.01 to 10 Seconds*. *Interim Report for USGS Review,* 219p, http://peer.berkeley.edu/lifelines/repngamodels.html (Last Accessed December 2006).

10. Boore, D.M., Joyner, W.B., and Fumal, T.E. (1997) Equations for estimating horizontal response spectra and peak accelerations from Western North American earthquakes: a summary of recent work. Seism. Res. Lett., **68**, 128-153.

11. Singh, R.P., Aman, A., and Prasad, Y.J. (1996) Attenuation relations for strong ground motion in the Himalayan region. *Pure and Applied Geophysics*, **147**(1), 161-180.

12. Garcia, D., Singh, S.K., Herraiz, M., Ordaz, M., and Pacheco, J. (2005) Inslab earthquakes of central Mexico: -Motion parameters and response spectra. *Bulletin of the Seismological Society of America*, **95**, 2272-2282.

13- Stromeyer, D. and Grünthal, G. (2009) Attenuation relationship of macroseismic intensities in central europe. *Bulletin of the Seismological Society of America*, **99**, 554 - 565.

14. Seed, H.B., Ugas, C., and Lysmer, J. (1976) Site-dependent spectra for earthquake-resistant design. *Bull. Seism. Soc. Am.*, **66**, 221-243.

15. Mohraz, B. (1976) A study of earthquake response spectra for different geological conditions. *Bull. Seism. Soc. Am.*, **66**, 915-935.

16. Steinbruooe, Karl V. (1970) 'Earthquake Damage and Structural Performance in the United States'. In: *Earthquake Engineering*, Weigel, R.L. (Ed.) Prentice-Hall, Englewood Cliffs, NJ.

17. Anderson, J.C and Naeim, R (1984) 'Design Criteria and Ground Motion Effects on Seismic Response of Multistory Buildings'. In: *Critical Aspects of Earthquake Ground Motion and Building Damage Potential*, ATC-10-l. Applied Technology Council, San Francisco, CA.

18. Anderson, J.C. and Bertero, V.V. (1987) Uncertainties in establishing design earthquakes. *J. of Structural Engineering*, ASCE, **113**(8), 1709-1724.

19. Boore, D.M., Joyner, W.B., Oliver, A.A. III, and Page, R.A. (1980) Peak acceleration velocity and displacement from strong motion records. *Bull. Seism. Soc. Am.*, **70**(1), 305-321.

20. Boore, D.M., Joyner, W.B. Oliver, A.A. III, and Page, R.A. (1987) Estimation of ground motion parameters. *United States Geological Survey*, Circular 795, Arlington, VA.

21. Borcherdt, R., Glassmouer, G. Andrews, M., and Cranswick, E. (1989) Effect of site conditions on ground motion and damage. *Earthquake Spectra, Special Supplement,* 23-42.

22. Anderson, J.G., Lee, Y. Zeng, Y., and Day, S. (1996) Control of strong motion by the upper 30 meters. *Bull. Seism. Soc. Am.*, **86**, 1749-1759.

23. Joyner, W.B. and Fumal, T.E. (1985) Predictive mapping of earthquake ground motion, in Evaluating Earthquake Hazards in the Los Angeles Region - An Earth-Science Perspective. J.E. Ziony (Ed.), U.S. Geol. Surv. Profess. Pap., 1360, 203-220.

24. Boore, D.M., Joyner, W.B., and Fumal, T.E. (1993) *Estimation of Response Spectra and Peak Accelerations from Western North American Earthquakes: An Interim Report*. U.S. Geol. Surv. Open-File Rept., 93-509.

25. Castro, R.R., Mucciarelli, M., Pacor, F., and Petrungaro, C. (1997) S-wave site-response estimates using horizontal-to-vertical spectral ratios. *Bull. Seism. Soc. Am.*, 87, 256-260.

26. IBC (2006) *The International Building Code*. International Code Council, Inc. United States Version

27. Ahmad, A.R. (2013) Seismic hazard assessment of Syria. *Journal of Seismology and Earthquake Engineering (JSEE)*, IIEES, **15**(1), 1-13.

28. Brew. G., Sawaf, T., Al-Maleh, K., and Barazangi, M. (2001) Tectonic and geologic evaluation of Syria. *GeoArabia, Gulf PetroLink, Bahrain*, **6**(4), 573-615.

29. Kattan, Z. (2006) Characterization of surface water and groundwater in the Damascus Ghotta basin: hydrochemical and environmental isotopes approaches. *Environ. Geol.*, **51**, 173-201.

30. Zaineh, H.E., Yamanaka, H., Dakkak, R., Khalil, A., and Daoud, M. (2012) Estimation of shallow S-wave velocity structure in damascus city, syria, using microtremor exploration. *Soil Dynamics and Earthquake Engineering*, **39**, 88-99.